Fractalization route to strange nonchaotic dynamics

Sandip Datta,[1] Ramakrishna Ramaswamy,[1] and Awadhesh Prasad[2]
[1]*School of Physical Sciences, Jawaharlal Nehru University, New Delhi 110067, India*
[2]*Department of Physics and Astrophysics, Delhi University, Delhi 110007, India*
(Received 15 January 2004; revised manuscript received 4 June 2004; published 11 October 2004)

In the fractalization route for the formation of strange nonchaotic attractors (SNA's) in quasiperiodically driven nonlinear dynamical systems, a smooth torus gradually becomes a fractal as the forcing amplitude is increased, while the Lyapunov exponent remains nonpositive. Using techniques introduced by Kim *et al.* to identify unstable sets in SNA's, we study torus fractalization in a sequence of approximations wherein the quasiperiodic drive is replaced by periodic forcing of increasing period. This allows us to identify an unstable set embedded in the attractor. In the periodically forced system, we show that there is a cascade of attractor merging crises, and argue that the quasiperiodic analogue of such crises causes fractalization of tori to create SNA's.

DOI: 10.1103/PhysRevE.70.046203 PACS number(s): 05.45.Ac

I. INTRODUCTION

Chaotic attractors occurring in low-dimensional dissipative systems usually have an intricate geometric structure in phase space: the capacity dimension of such an attractor often assumes noninteger values. These are termed strange [1]. In 1984, Grebogi *et al.* [2] constructed systems where the dynamics was on fractal attractors but was also *nonchaotic*, namely, the largest Lyapunov exponent was negative (or zero, at most). The infinitesimal fine scale structure similar to strange sets combined with the lack of sensitivity to initial condition are characteristic of strange nonchaotic attractors (SNA's) [3].

The term fractalization was first used to describe the phenomenology of the dynamics in a study of the quasiperiodically driven quadratic map by Kaneko [4] who observed that with increasing forcing, the torus attractors of the (two-dimensional) mapping became increasingly wrinkled, eventually turning fractal at a critical point. There also was an interruption of the period-doubling cascade with an accelerated transition to chaos. In a subsequent and more detailed study, Nishikawa and Kaneko [5] showed that this process leads to strange nonchaotic dynamics and termed this the fractalization route to SNA.

Although by now it is known that SNAs are typical in quasiperiodically forced systems—in that they can occur in a set of nonzero Lebesgue measure in the parameter space, intermediate between ordered and chaotic motion—all bifurcations and mechanisms leading to such dynamics have not been completely characterized. Quasiperiodic extensions of the bifurcations that commonly occur in nonlinear dynamical systems underlie most of the known scenarios for the formation of SNA's [3]. It should be noted that while it is possible to find fractal nonchaotic attractors in systems which are not quasiperiodically forced, these are neither typical nor robust to perturbations. Several routes leading to the formation of SNA's are known [6–11], although there are few rigorous results available [12–15] which establish both the fractal and the nonchaotic properties for most such cases.

An essential feature of SNA's is the existence of an unstable set embedded within the attractor. This follows from the results of Stark [16] and Sturman and Stark [17], who proved that a strange compact invariant set for quasiperiodically forced systems must support at least one invariant measure with non-negative maximal Lyapunov exponent. Thus the attractor contains locally unstable regions even though globally the dynamics is nonchaotic. Such locally unstable regions can be characterized by studying the local Lyapunov exponents [18] which can be positive on an SNA depending on initial conditions. Distributions of local Lyapunov exponents have proved to be useful in characterizing SNA's [19].

The fractalization route to SNA is one which is not associated with a specific bifurcation, unlike the other known scenarios for the formation of such attractors [3]. Though it is clear that there must be an unstable component to the attractor, it has not proved to be straightforward to identify this set.

In this paper we examine the process of fractalization and demonstrate that a cascade of attractor merging crises precedes the creation of the fractal attractor. We follow the method used by Kim, Lim, and Ott [10] to find unstable sets for the fractalization process using a sequence of rational approximations (RA's) [20]. These unstable sets are created through a cascade of period-doubling bifurcations, and collision of chaotic bands with them causes a cascade of interior merging crises whereby the fractalization process takes place.

We study both quasiperiodically driven mappings such as the forced logistic map (in Sec. II), as well as continuous systems such as the forced Duffing oscillator (in Sec. III). In either case, it is necessary to analyze a sequence of periodically forced systems that approximate the quasiperiodic system. These two models have been extensively studied with regard to the creation of SNA via fractalization [5,21]; we thus believe the mechanism which we elucidate for the creation of fractalized SNA's to be quite generally applicable. The paper concludes with a discussion and summary in Sec. IV.

II. THE FORCED LOGISTIC MAP

Commonly studied examples of forced dynamical systems have been skew product maps

$$x_{n+1} = f(x_n, \theta_n), \tag{1}$$

$$\theta_{n+1} = \omega + \theta_n \mod 1, \tag{2}$$

where the forcing variable θ evolves by rigid rotation. When ω is irrational, the forcing is quasiperiodic, and for a variety of such systems, SNA's have been observed for a range of parameter values in the vicinity of transition to chaos [5,7,10,21]. Unlike chaotic attractors, SNA's do not show sensitivity to initial conditions, but there is sensitivity to the *phase* variable [18], namely, θ, and to the forcing amplitude (or system parameters) [5]. The origin of this phase sensitivity arises from the fact that even though the asymptotic Lyapunov exponent is nonpositive, the local Lyapunov exponents can remain positive for long time intervals for typical orbits on SNA's [18].

Following Nishikawa and Kaneko [5], we describe the phenomenology of fractalization in the logistic map with additive quasiperiodic forcing, namely, the case of

$$x_{n+1} = f(x_n, \theta_n) = \alpha x_n(1 - x_n) + \epsilon \sin(2\pi\theta_n) \tag{3}$$

with $\omega = (\sqrt{5}-1)/2$. In Eqs. (2) and (3) at zero forcing, namely, $\epsilon = 0$, the logistic map has a single attracting fixed point for $1 \leqslant \alpha \leqslant 3$. Thus, for example, at $\alpha = 3$, the attractor for the above system is a one torus which is a straight line in the phase space (x, θ). With increasing ϵ this one torus develops curvature (while remaining a smooth closed curve), and eventually becomes a SNA at $\epsilon \sim 0.1553$ [5]. At higher values of ϵ the stability along the x direction is lost and the fractal nonchaotic attractor is replaced by a chaotic attractor, above $\epsilon \sim 0.1573$. Nishikawa and Kaneko [5] verify the existence of SNA for $0.1553 \leqslant \epsilon \leqslant 0.1573$ by showing that the attractor has noninteger dimension and that the dynamics has phase and parameter sensitivity.

Extending this calculation, we obtain the phase diagram for the forced logistic map, shown in Fig. 1(a). We have found it useful to characterize the dynamics through both the Lyapunov exponent λ_x, which is given by

$$\lambda_x = \lim_{N\to\infty} \frac{1}{N} \sum_{i=1}^{N} \ln \left| \frac{\partial f(x_i, \theta_i)}{\partial x_i} \right| \tag{4}$$

and the phase sensitivity exponent which can be obtained from phase sensitivity function Γ_N [18]

$$\Gamma_N(\alpha, \epsilon) = \min_{x_0, \theta_0} \left(\max_{0 \leqslant n \leqslant N} \left| \frac{\partial x_n}{\partial \theta} \right| \right). \tag{5}$$

On a SNA, the function Γ_N grows with the length of the orbit N, as a power, i.e., $\Gamma_N \sim N^{\gamma}$, where γ is the phase sensitivity exponent [18]. (Although we have not used it here, the parameter sensitivity exponent [5] has a similar behavior.) Regular motion [the white region in Fig. 1(a)] is characterized by a negative Lyapunov exponent and zero phase sensitivity exponent. SNA (the colored regions) dynamics has $\gamma \neq 0$ and negative λ_x, while chaotic motion (the black region) has $\gamma \neq 0, \lambda_x > 0$.

SNA's in the quasiperiodically forced logistic map appear through various routes [22]. Indicated in Fig. 1(a) are the regions in parameter space where the fractalization mechanism operates (F), the narrow region corresponding to the intermittency scenario (I), and the region where SNA's are created through torus collision (TC). As has been extensively discussed [3,22], all these routes are dynamically distinct.

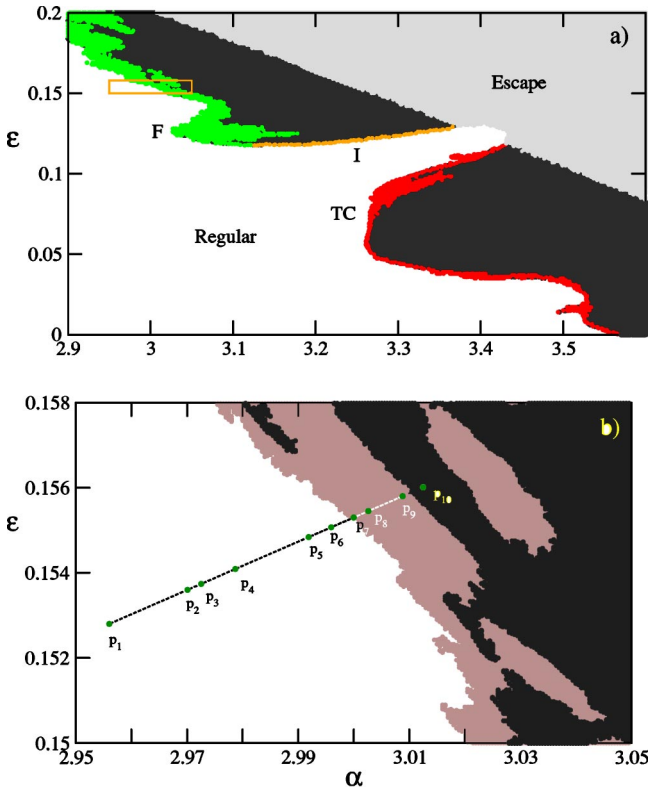

FIG. 1. (Color online) (a) Phase diagram of the forced logistic map computed for a set of 250×250 points in the α-ϵ plane. Regular, chaotic, SNA, and escape regions are shown by white, black, colored (red, yellow, and green) , and light gray, respectively. SNA's are formed through the fractalization (labeled by F), intermittency (I), and torus collision (TC) routes. (b) A blowup of the boxed region of the phase diagram shown in (a). The path chosen for study approaches the SNA region approximately normally and is indicated by the dashed line. The coordinates of the various indicated points are $p_1 = (2.956, 0.1528)$, $p_2 = (2.97008, 0.1536)$, $p_3 = (2.972544, 0.15374)$, $p_4 = (2.978704, 0.15409)$, $p_5 = (2.991904, 0.15484)$, $p_6 = (2.995952, 0.155507)$, $p_7 = (3, 0.1553)$, $p_8 = (3.00264, 0.15545)$, $p_9 = (3.0088, 0.1558)$, and $p_{10} = (3.0125, 0.15601)$.

We focus on a small portion of this parameter space where all SNA's that occur are created through fractalization. Shown in Fig. 1(b) is an expansion of the boxed region in Fig. 1(a); this includes the parameter range studied by Nishikawa and Kaneko [5]. Note that the boundaries of the regular-SNA-chaotic regions in the phase plane are also likely to be fractal, although this has not been conclusively established at the present level of computational effort.

A. Fractalization path

The mechanism of fractalization can be understood more clearly if we approach the SNA region along a line which is normal to the boundary, namely, by varying both parameters

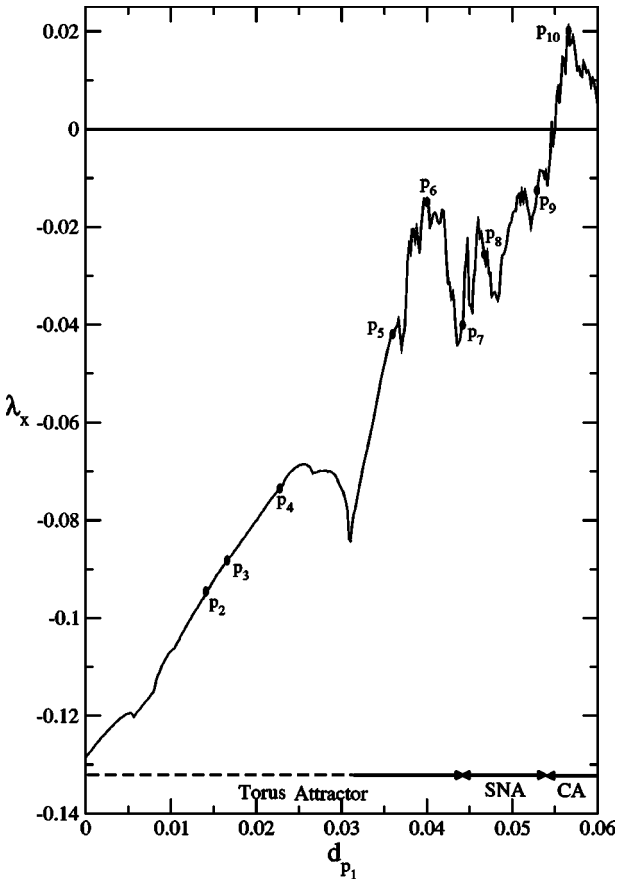

FIG. 2. The nontrivial Lyapunov exponent calculated along the dotted line on the parameter plane shown in Fig. 1(b) from 10^6 points, discarding the initial 10^4 as transients. The abscissa is the distance of various points from p_1, denoted by d_{p_1}. The regions of torus, SNA and chaotic attractor (CA) are indicated on the horizontal line at the bottom of the figure.

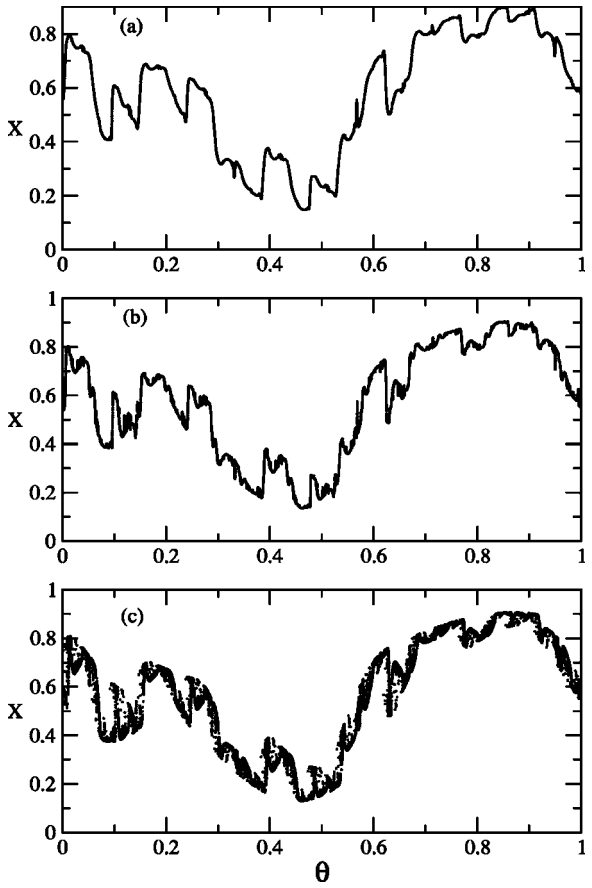

FIG. 3. The attractor of the dynamics along the fractalization path at (a) p_4, (b) p_6, and (c) p_8.

α and ϵ. The path we follow here is indicated in Fig. 1(b) joining points $p_1 \cdots p_{10}$ and the variation of Lyapunov exponent λ_x along this line is shown in Fig. 2. (The other Lyapunov exponent for the system is zero since the θ dynamics is a rotation.) The attractor at p_4 is a smooth torus, and at p_6, near the SNA region, it becomes wrinkled as shown in Fig. 3. The SNA obtained through fractalization route is shown in Fig. 3(c) corresponding to p_8 where the transition to the fractalized SNA is complete. At p_{10}, λ_x is positive; the system is chaotic.

In order to locate the unstable set embedded in the attractor we use a standard method to approximate the irrational drive frequency ω by an increasingly accurate series of rational numbers [8,10,20,23]. These are the convergents in the continued fraction representation of ω, and for the inverse golden mean ratio that we use here, namely $\omega=(\sqrt{5}-1)/2$, they are ratios of successive Fibonacci numbers. Thus we approximate ω by $\omega_k=F_{k-1}/F_k$, where $F_{k+1}=F_k+F_{k-1}$ with $F_0=0$ and $F_1=1$.

B. Rational approximations

When the irrational ω in Eq. (2) is replaced by its rational approximation ω_k, one necessarily has a periodically forced system which approaches the original quasiperiodic case in the limit $k \to \infty$. The driven system with $\omega=\omega_k=F_{k-1}/F_k$ is termed the rational approximation of order k.

Depending on the initial phase θ_0, the *periodically* forced logistic map has either periodic or chaotic attractors. Due to the periodicity it is sufficient to restrict θ_0 to the interval $[0,1/F_k]$; the remainder of the attractor can be obtained by iterating these values F_k-1 times. The kth order approximation to the attractor of the quasiperiodically forced system is thus the union of all attractors for $0 \leqslant \theta_0 \leqslant 1$. The attractor for the rational approximation of level 6 at the point p_5 is shown in Fig. 4(a). Also shown, superimposed in gray, is the unstable set, which we obtained using the methods outlined in Kim, Lim, and Ott [10]. The attractor in Fig. 4(a) is composed of 7 ($\equiv F_6-1$) evolved iterates of the attractor within the window (shown by boxed region in the figure). This basic window is rescaled and displayed in Fig. 4(b). Since the qualitative features are unchanged in each of the copies, we restrict attention to the attractor in $[0,1/F_k]$ henceforth.

For fixed α and ϵ, the initial phase θ (henceforth we drop the subscript for simplicity) can be regarded as a bifurcation parameter [10], and hence the attractor of the dynamics can be interpreted as a bifurcation diagram. Note that as a function of θ, there is a period doubling bifurcation where a stable orbit bifurcates into a stable period-two orbit, and one unstable orbit. At a subsequent value of θ, there is a reverse period-doubling bifurcation where the period-two orbits

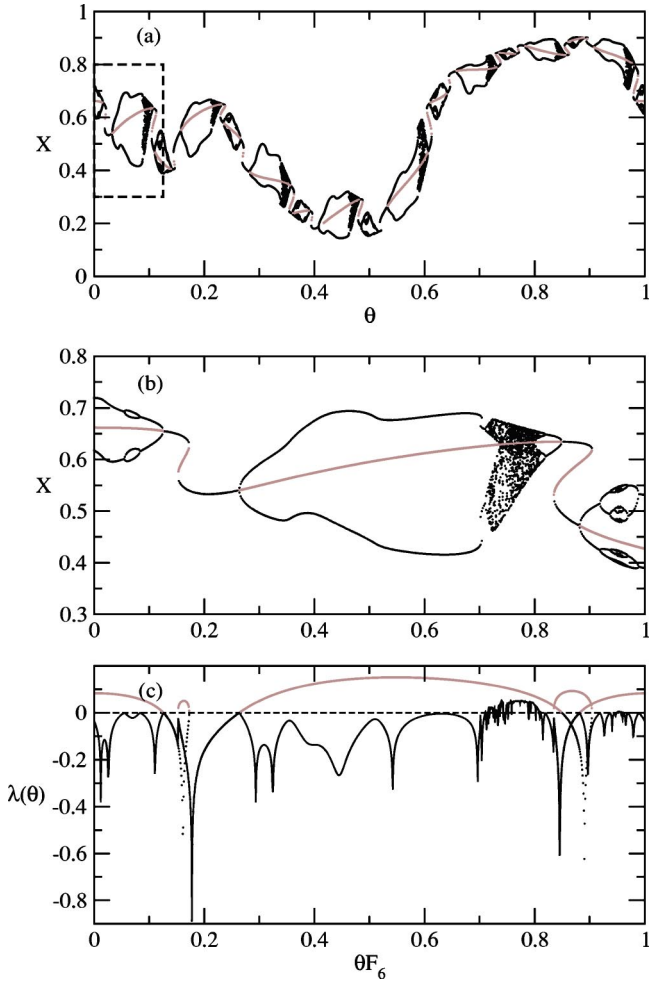

FIG. 4. (Color online) For the rational approximation of order 6, namely, $\omega_k = 5/8$, (a) the stable set (marked by dots) and the unstable set (the light pink line) calculated at the point p_5 on the parameter plane [see Fig. 1(b)]. (b) Enlargement of the dashed portion of (a), showing the stable and unstable sets (light pink line). (c) The Lyapunov exponent corresponding to the stable and the unstable set (in black and light pink, respectively). Note the change of scale in θ in (b) and (c).

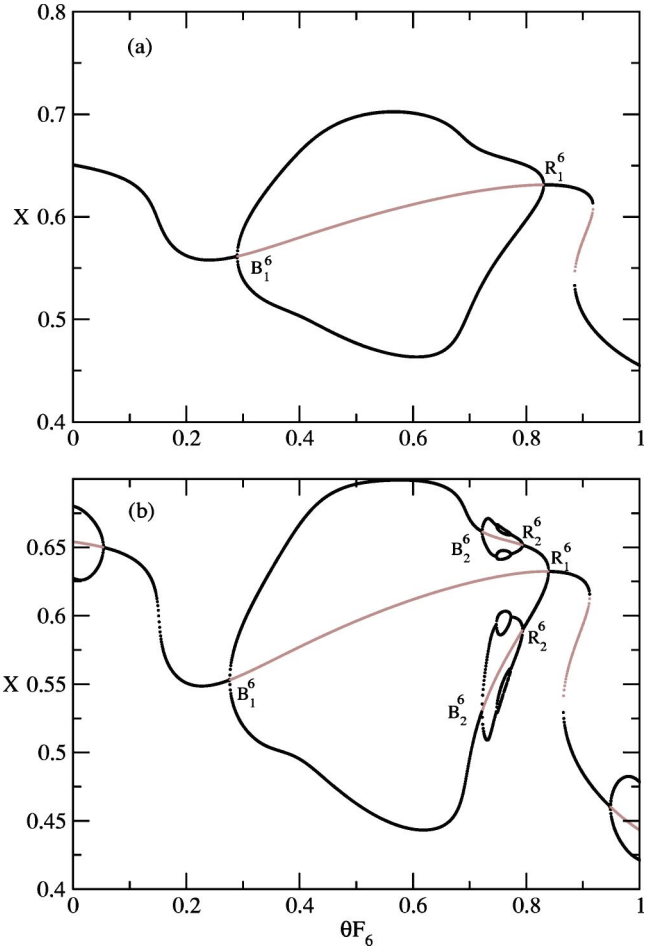

FIG. 5. (Color online) For the rational approximation of order 6, namely, $\omega_k = 5/8$, the attractor along with the ustable set (in light pink) at (a) p_1 and (b) p_2.

merge to form a period-one orbit. The structures apparent in Fig. 4(b) are composed of a series of period-doubling bifurcations and reverse period-doubling bifurcations within the so-called "bubble" bifurcation plots. Essentially as a function of θ, one can have a period-doubling bifurcation, which (because of continuity at the window boundary) must be reflected in a reverse bifurcation. These period-doubling bifurcations accumulate in a transition to a chaotic attractor, and as is common, will result in a sequence of band mergings. This appears eventually as a chaotic band delimited on both sides by a period-doubling cascade, and the periodic part of the stable set contains components of period $2^m F_k$, $m = 0, 1, 2, \ldots$.

When ω is approximated by its kth order rational approximation, one can define a Lyapunov exponent for each initial θ using Eq. (4), however, with ω_k in the dynamical equation (2). Depending on whether the initial θ corresponds to the chaotic, quasiperiodic or periodic ranges of the attractor, $\lambda_x^{(k)}(\theta)$ will be greater than, equal to, or less than zero. Now following Kim, Kim, Hunt, and Ott [23], the order k Lyapunov exponent $\lambda_x^{(k)}$ for the orbit can be defined as [23]

$$\lambda_x^{(k)} = \int_0^1 \lambda_x^{(k)}(\theta) d\theta \tag{6}$$

by integrating over all initial θ. In the limit of $k \to \infty$, $\omega_k \to \omega$, and clearly $\lambda_x^{(k)} \to \lambda_x$ [see Eq. (4)].

Shown in Fig. 4(c) is $\lambda_x^{(6)}(\theta)$ [see Fig. 4(b)] for both the stable and the unstable sets. There is a smooth variation of the order k Lyapunov exponent for the unstable periodic orbits for which the Lyapunov exponent is always positive, and a comparatively nonsmooth variation of the same for θ values when the attractor is chaotic.

The basic mechanism of the fractalization process can be understood from the transitions occurring along the path from p_1 to p_4 in the parameter plane of Fig. 1(b) at successive orders of rational approximations. Introducing the notation B_j^k to denote the bifurcation to period 2^j orbits in the rational approximation of order k, we show in Fig. 5(a) the bifurcation B_1^6, when there is a period-doubling bifurcation giving an unstable orbit of period F_6 and a stable orbit of

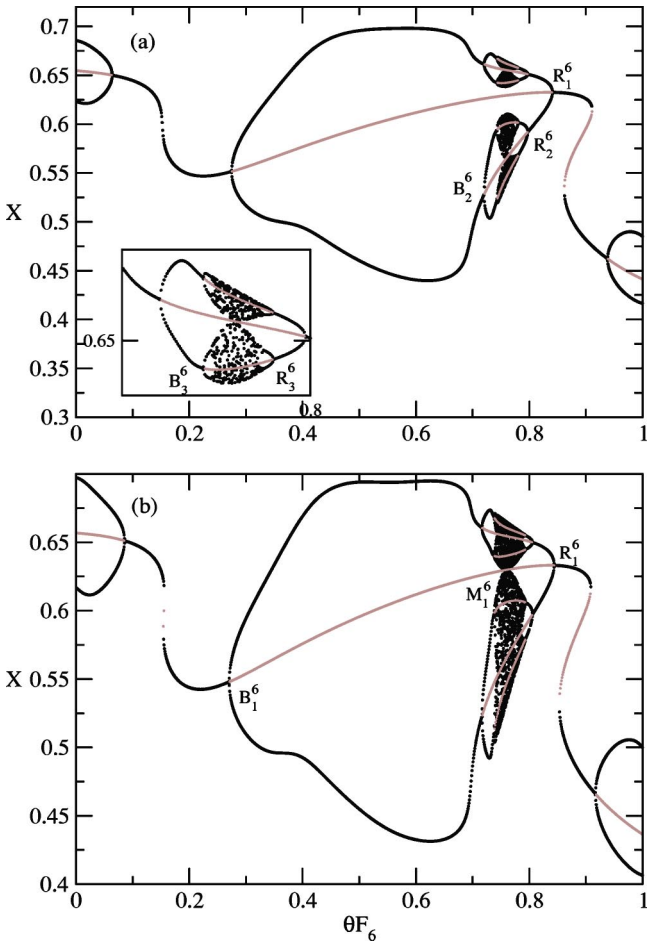

FIG. 6. (Color online) As in Fig. 5, at (a) p_3 and (b) p_4.

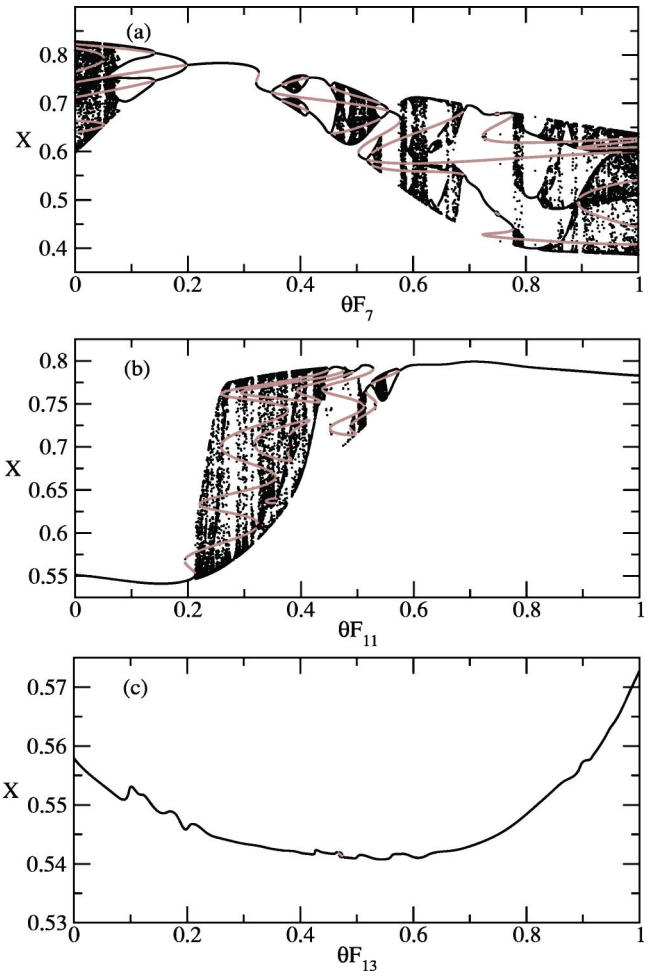

FIG. 7. (Color online) The rational approximations to the quasiperiodic attractors at various orders, at the point p_6. The stable and unstable sets are denoted by black and light pink dots, respectively. (a) Order 7, $\omega_7=8/13$. (b) Order 11, $\omega_{11}=55/89$. (c) Order 13, $\omega_{13}=144/233$. Note that p_6 lies outside the SNA region, and the chaotic component vanishes at order 13, leaving, as a remnant of the bifurcations, the small bubble in (c).

period $2F_6$. This is followed by a reverse bifurcation R_1^6 whereby the orbit of period F_6 becomes stable again. With increasing parameters, at point p_2 along the path, the bifurcations B_1^6, B_2^6, and B_3^6 are shown in Fig. 5(b) giving unstable orbits, in different ranges of θ, of periods F_6, $2F_6$, and 2^2F_6. With changing parameter values a cascade of such bifurcations follow, giving unstable and stable orbits of all periods 2^nF_k, $n=1,2,3,\ldots$, in successively smaller windows in θ, and eventually giving rise to a chaotic component as is clearly visible in Fig. 6.

At p_3 [see Fig. 6(a)] the dynamics is chaotic for a range of θ, flanked on both sides by a period-doubling cascade. There are two such chaotic bands with an unstable orbit of period F_6 between. As the point p_4 is approached, these two chaotic attractors collide simultaneously with the unstable period F_6 orbit. An attractor merging crises takes place as shown in Fig. 6(b). We term this M_1^6. Each chaotic attractor which merges through interior or merging crises was born through a similar process, as can be seen in Fig. 6(a) where the four chaotic windows just touch the unstable period $2F_6$ orbits; this is the merging M_2^6. In the inset of Fig. 6(a) the upper chaotic band is magnified, showing the earlier band-merging crises where chaotic attractors have already collided with period 2^nF_6 unstable orbits. Three such bubbles at various stages of development are visible in Fig. 4(b). With further increase of the parameter values the number of such cascades increases.

C. Asymptotics

The sequences of bifurcations and reverse bifurcations depend on both the parameter values (namely, α and ϵ) as well as the order of the rational approximation. Thus, for low k, far into the regular region, one typically observes the truncated sequences

$$B_1^k, B_2^k, \ldots, B_m^k, R_{m-1}^k, \ldots, R_2^k, R_1^k \tag{7}$$

with finite m. When the transition is made to chaotic dynamics within the rational approximation, then the sequence of

$$B_1^k, B_2^k, \ldots, B_\infty^k \equiv M_\infty^k, \ldots, M_j^k, \ldots, R_2^k, R_1^k \tag{8}$$

for $j \geqslant 1$ can obtain. With increasing k, if the parameters are in the regular region, then the bifurcation sequence of Eq. (7) eventually obtains, whereas if the parameters correspond to the SNA or chaotic regime, then the sequence (8) is realized.

In Fig. 7 at the point p_6 on the parameter plane (which lies just outside the SNA region) the rational approximation to

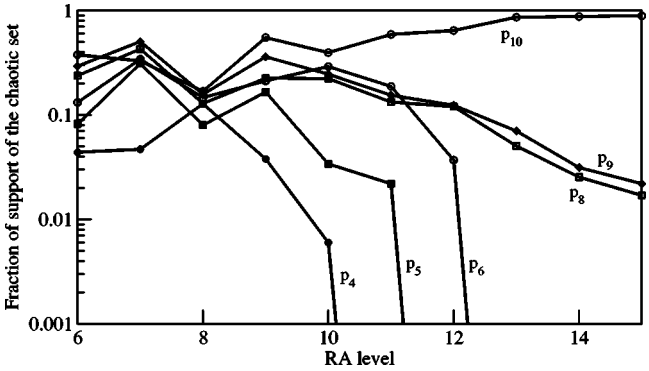

FIG. 8. The support of the chaotic part of the attractor with the increasing order of rational approximation, calculated for 5000 initial θ. When this asymptotically goes to zero, a nonstrange nonchaotic attractor results. For strange attractors, there is always a residual chaotic set at any order of rational approximation. At the point p_{10}, the attractor of the quasiperiodically forced system is chaotic.

the attractor at various orders is shown. The chaotic component is seen to keep decreasing with the increase of order, and [see Fig. 7(c)] vanishes for $k \geqslant 13$. Since the full attractor at $k=13$ is composed of 377 evolved copies of this attractor, we infer that the torus is indeed "wrinkled," but in the $k \to \infty$ limit does not become a fractal. Note that for the rational approximation of order 13 the sequence of bifurcations $B_1^{13}R_1^{13}$ is visible in a small range of θ, corresponding to the scenario (7).

This scenario can be quantitatively characterized by measuring the chaotic component of the dynamics—the width of the intervals in θ that give a positive Lyapunov exponent [see Eq. (6)]—as a function of the rational approximation order k. This will eventually go to zero for regular (torus) dynamics, whereas for SNA or chaotic motion, this quantity will asymptote to a constant. This quantity, at different points along the fractalization path, is shown in Fig. 8. At p_4, which is outside the SNA region, the fraction of chaotic component vanishes for the order 11 rational approximation, while at p_6 which is just at the threshold of the SNA region, a measurable fraction of initial θ lead to chaotic dynamics even for the order 15 rational approximation. In the SNA region, at point p_8 and beyond, the measure of the surviving chaotic component remains nonzero for all orders of the rational approximation. In our numerical simulations we have found that the support of the chaotic component appears to have a nonmonotonic variation with respect to the increase of order of rational approximation, but this is likely to arise from the fact that the boundaries of various dynamical regions are themselves probably fractal.

Whether the attractor is nonchaotic or chaotic depends on the surviving fraction of the chaotic component. When asymptotically there is no surviving chaotic component, the attractor is clearly nonchaotic and will be a wrinkled torus. At the transition to SNA, the fraction of chaotic motion that survives at each order of the rational approximation is enough to contribute some instability to the motion and confer fractality to the attractor without making the Lyapunov exponent positive. At the transition point from SNA to chaos, the total positive Lyapunov exponent corresponding to the chaotic component balances the total negative Lyapunov exponent coming from the regular component. When, as at the point marked p_{10} in Fig. 1(b), the chaotic component is larger than the regular, the global Lyapunov exponent becomes positive and results in a fractal chaotic attractor. As can be seen in Fig. 8, for p_{10} the fraction of the chaotic component approaches unity with increasing order of the rational approximation.

III. THE FORCED DUFFING OSCILLATOR

The scenario that has been described in the previous section appears to apply quite generally. Here we study the fractalization route to SNA in a continuous system, the quasiperiodically forced Duffing oscillator. A variant of this system can be realized in experiment as the magnetoelastic ribbon; indeed this was one of the first systems where SNA's were observed [24]. Such continuous-time-dynamical systems can also be reduced to mappings via the Poincaré section technique.

The equation of motion for the quasiperiodically forced Duffing oscillator [21,24,25] is

$$\ddot{x} + h\dot{x} - [1 + A(R\cos t + \cos \omega t)]x + x^3 = 0, \tag{9}$$

where the frequency ω is taken to be an irrational number, h is the damping constant, and A and R determine the coupling and amplitude of the quasiperiodic forcing term. This can be rewritten as a set of autonomous coupled first-order differential equations

$$\dot{x} = y, \tag{10}$$

$$\dot{y} = [1 + A(R\cos\phi + \cos\theta)]x - x^3 - hy, \tag{11}$$

$$\dot{\phi} = 1, \tag{12}$$

$$\dot{\theta} = \omega \tag{13}$$

in a four-dimensional phase space. Earlier studies of the forced Duffing oscillator [21,25] have established that with quasiperiodic forcing SNA's are created through several different mechanisms, including fractalization. A detailed study of these routes has been presented earlier in Ref. [21] where phase diagrams describing the different dynamical behavior as a function of the different parameters has also been given.

We restrict attention to the portion of the parameter region where the fractalization transition to SNA is known to occur [21], namely, for $\omega=(\sqrt{5}+1)/2$, $h=0.0552$, and $A=0.3$. Equation (9) is numerically integrated with a fourth-order Runge-Kutta algorithm with step size 0.01 in natural units. The Lyapunov exponents are computed as a function of the parameter R.

Shown in Fig. 9 is the largest nontrivial Lyapunov exponent as a function of R. At the points p_1 and p_2 the dynamics is regular; the attractor at p_2 is shown in Fig. 10(a) projected onto the (x,θ) plane. Near p_3, there is a transition from regular motion to SNA via the fractalization route. p_4 lies in the

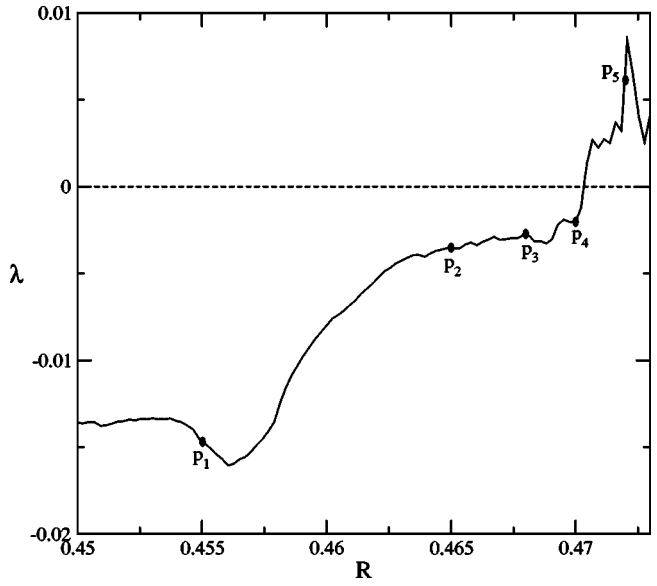

FIG. 9. The largest nontrivial Lyapunov exponent as a function of the parameter R, for $h=0.552$ and $A=0.3$, for the forced Duffing oscillator. The values of R at points $p_i, i=1,\ldots,5$ are 0.455, 0.465, 0.468, 0.47, and 0.472.

SNA region: the corresponding attractor is shown in Fig. 10(b). At p_5 the largest Lyapunov exponent is positive and the dynamics is chaotic.

The rational approximation technique to investigate the transition from regular motion to SNA involves replacement of the irrational driving frequency ω by $\omega_k=F_k/F_{k-1}$ at order k, where the F_k's are the Fibonacci numbers. As in the case of the mapping studied in the previous section, the initial value of the phase variable θ becomes a bifurcation parameter, and depending on the initial phase the attractor of the periodically driven Duffing oscillator can be regular or chaotic.

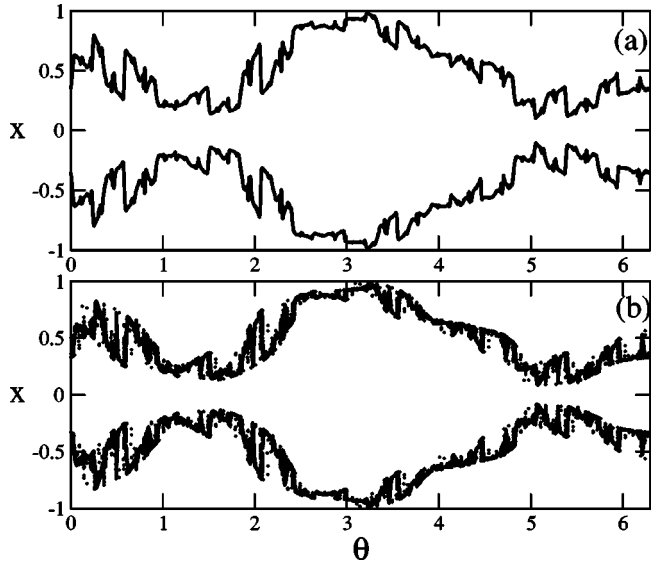

FIG. 10. Projection of the two-frequency torus attractor of the forced Duffing oscillator on the (x,θ) plane at (a) p_2 and (b) p_4. The first 10^5 iterates are discarded and the subsequent 50 000 points have been plotted.

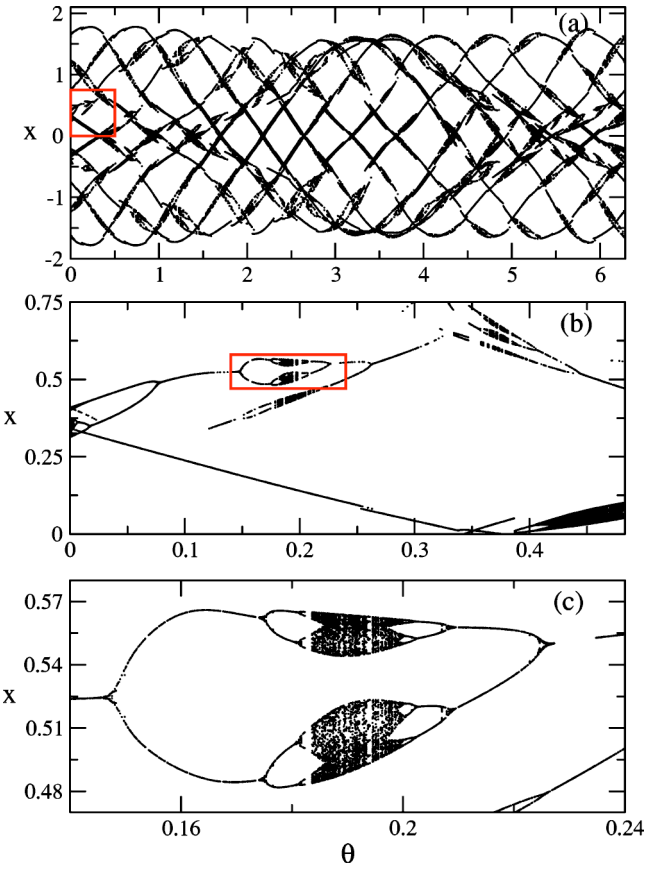

FIG. 11. (Color online) (a) Poincaré section of the attractor of the dynamics for the forced Duffing oscillator with periodic forcing, $\omega=13/8$ at the point p_1 ($R=0.455$). The boxed region in (a) is expanded in (b), and the boxed region in (b) is expanded in (c). Since the asymptotic attractor (with irrational ω) is a quasiperiodic torus, the chaotic component of the attractor will diminish with increasing order of rational approximation.

The analysis here parallels that presented in Sec. II since the mechanism of fractalization in the forced Duffing system is very similar to that in the forced logistic map. At a given level of rational approximation, a cascade of period doublings are followed by cascade of mergings. Shown in Fig. 11(a) is the periodic attractor for $\omega=F_7/F_6=13/8$. Succesive expansion of this figure reveals additional features in the bifurcation diagram: the period doublings and the band mergings are clear in Figs. 11(b) and especially 11(c), where the merging M_2^6 has already taken place [compare with Figs. 4(a) and 4(b)].

By choosing different intermediate values of R, the entire set of bifurcations and reverse bifurcations analogous to those shown in Figs. 5–7 for the forced logistic map can be located. The fraction of initial θ values that lead to chaotic dynamics can also be computed at each order of the rational approximation. As in the case of the forced logistic map, the fraction of the chaotic component decreases and eventually vanishes for parameters corresponding to quasiperiodic torus attractors (p_1 and p_2, for instance), while it asymptotes to a nonzero fraction when the limiting attractor is fractal (at p_3, p_4, and p_5), as shown in Fig. 12. The distinction between SNA's and chaotic fractal attractors appears to be in the ex-

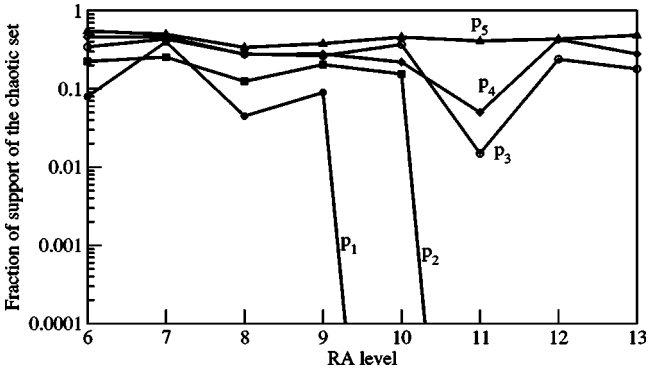

FIG. 12. Variation of the support of the chaotic part of the attractor with the increasing order of rational approximation for the forced Duffing oscillator at points $p_1, \ldots, p_5$; see Fig. 9. p_1 and p_2 are in the torus regime, p_3 and p_4 are in the fractalized SNA region, and at p_5 there is a chaotic attractor.

tent of chaotic dynamics asymptotically. At p_5, when the resulting attractor is chaotic, namely, with positive Lyapunov exponent, the fraction of θ leading to chaotic motion approaches 1.

IV. SUMMARY

In the past few years a number of different scenarios for the formation of SNA's have been described [3]. The recognition that there is necessarily an interplay between local unstable dynamics and global stability requires the identification of an unstable set that is embedded within the attractor [17]. In the torus collision scenarios, such as those described by Heagy and Hammel [6] or by Pikovsky and Feudel [18], the interaction between stable and unstable tori that lead to the SNA makes such an identification obvious. For other routes, such as the blowout bifurcation [2,9], the available results [12,13] are also in consonance with the same feature. Kuznetsov [26] has also discussed the transformation of a smooth invariant curve to a fractal attractor when there is a saddle-node bifurcation in the presence of quasiperiodic forcing. For a particular case, the renormalization group analysis has been carried out, and a transition to SNA is reported, resulting, however, from the collision of an attractor and a repeller at a fractal set of points [26]; the unstable embedded set is easily identified.

The fractalization [5] and the intermittency routes [7] to SNA present instances where the location of unstable set is possible only through a detailed examination of a sequence of periodic approximations to the quasiperiodic motion [10,27]. For the intermittency route, a ring shaped unstable set which is created via the quasiperiodic analogue of tangent bifurcations can be identified [10]. Collision of a quasiperiodic torus with this unstable set gives rise to the chaotic component responsible for the transition to SNA's.

In this paper we have adapted the method of Kim *et al.* [10] to address the problem of formation of SNA's via fractalization. Application has been made to two representative examples of quasiperiodically forced dynamical systems: the logistic map, which has been a testing ground for initial studies of SNA's [4,6,23], and the Duffing oscillator [21], which has the added advantage of allowing experimental realization [24]. Using successive rational approximations, it has been possible to locate the unstable sets embedded in the attractor. These take the form of disjoint lines, and are the analogs of unstable periodic orbits appearing at period-doubling bifurcations. The cascade of bifurcations as this unstable set collides with chaotic bands through band-merging crises is the basic mechanism underlying fractalization. With the increase of order of rational approximation the chaotic component keeps decreasing and eventually vanishes at high order for points which lie in the regular region of the parameter plane. In the SNA region, for a finite measure of θ values, the attractor remains chaotic even at high orders of the periodic approximation. Though this chaotic set is not dense in the whole θ interval, in the quasiperiodic limit, any finite chaotic component will be distributed uniformly and ergodically, and therefore the torus is *fractalized*.

ACKNOWLEDGMENTS

This work was supported by a grant from the Department of Science and Technology. S.D. and R.R. would like to thank Professor S.-Y. Kim for helpful correspondence.

[1] J. P. Eckmann and D. Ruelle, Rev. Math. Phys. **57**, 617 (1985).
[2] C. Grebogi, E. Ott, S. Pelikan, and J. Yorke, Physica D **13**, 261 (1984).
[3] A. Prasad, S. S. Negi, and R. Ramaswamy, Int. J. Bifurcation Chaos Appl. Sci. Eng. **11**, 291 (2001).
[4] K. Kaneko, Prog. Theor. Phys. **71**, 1112 (1984).
[5] T. Nishikawa and K. Kaneko, Phys. Rev. E **54**, 6114 (1996).
[6] J. F. Heagy and M. S. Hammel, Physica D **70**, 140 (1994).
[7] A. Prasad, V. Mehra, and R. Ramaswamy, Phys. Rev. Lett. **79**, 4127 (1997).
[8] U. Feudel, J. Kurths, and A. S. Pikovsky, Physica D **88**, 176 (1995).
[9] T. Yalcinkaya and Y. C. Lai, Phys. Rev. Lett. **77**, 5039 (1996).
[10] S.-Y. Kim, W. Lim, and E. Ott, Phys. Rev. E **67**, 056203 (2003).
[11] V. S. Anishchenko, T. E. Vadivasova, and O. Sosnovtseva, Phys. Rev. E **53**, 4451 (1996).
[12] G. Keller, Fundam. Math. **151**, 139 (1996).
[13] Z. I. Bezhaeva and V. I. Oseledets, Funct. Anal. Appl. **30**, 223 (1996).
[14] J. Ketoja and I. I. Satija, Physica D **109**, 70 (1997).
[15] A. Prasad, R. Ramaswamy, I. I. Satija, and N. Shah, Phys. Rev. Lett. **83**, 4530 (1999).
[16] J. Stark, Physica D **109**, 163 (1997).
[17] R. Sturman and J. Stark, Nonlinearity **13**, 113 (2000).
[18] A. S. Pikovsky and U. Feudel, Chaos **5**, 253 (1995).

[19] A. Prasad and R. Ramaswamy, in *Nonlinear Dynamics: Integrability and Chaos*, edited by M. Daniel, K. Tamizhmani, and R. Sahadevan (Narosa, New Delhi, 2000), pp. 227–34.
[20] J. M. Greene, J. Math. Phys. **20**, 1183 (1979).
[21] A. Venkatesan, M. Lakshmanan, A. Prasad, and R. Ramaswamy, Phys. Rev. E **61**, 3641 (2000).
[22] A. Prasad, V. Mehra, and R. Ramaswamy, Phys. Rev. E **57**, 1576 (1998).
[23] J. Kim, S.-Y. Kim, B. Hunt, and E. Ott, Phys. Rev. E **67**, 036211 (2003).
[24] W. L. Ditto, M. L. Spano, H. T. Savage, S. N. Rauseo, J. Heagy, and E. Ott, Phys. Rev. Lett. **65**, 533 (1990).
[25] J. F. Heagy and W. L. Ditto, J. Nonlinear Sci. **1**, 423 (1991).
[26] S. P. Kuznetsov, Phys. Rev. E **65**, 066209 (2002).
[27] B. Hunt and E. Ott, Phys. Rev. Lett. **87**, 254101 (2001).